Microstructure and transport properties of ZnO:Mn diluted magnetic semiconductor thin films

Z. Yang,[1] W. P. Beyermann,[2] M. B. Katz,[3] O. K. Ezekoye,[3] Z. Zuo,[1] Y. Pu,[2] J. Shi,[2] X. Q. Pan,[3] and J. L. Liu[1,a)]
[1]*Department of Electrical Engineering, Quantum Structures Laboratory, University of California, Riverside, California 92521, USA*
[2]*Department of Physics and Astronomy, University of California, Riverside, California 92521, USA*
[3]*Department of Materials Science and Engineering, University of Michigan, Ann Arbor, Michigan 48109, USA*

(Received 16 September 2008; accepted 21 January 2009; published online 9 March 2009)

Microstructural studies using transmission electron microscopy were performed on a ZnO:Mn diluted magnetic semiconductor thin film. The high-resolution imaging and electron diffraction reveal that the ZnO:Mn thin film has a high structural quality and is free of clustering/segregated phases. High-angle annular dark field imaging and x-ray diffraction patterns further support the absence of phase segregation in the film. Magnetotransport was studied on the ZnO:Mn samples, and from these measurements, the temperature dependence of the resistivity and magnetoresistance, electron carrier concentration, and anomalous Hall coefficient of the sample is discussed. The anomalous Hall coefficient depends on the resistivity, and from this relation, the presence of the quadratic dependence term supports the intrinsic spin-obit origin of the anomalous Hall effect in the ZnO:Mn thin film. © *2009 American Institute of Physics*. [DOI: 10.1063/1.3087473]

I. INTRODUCTION

In recent years, ZnO-based diluted magnetic semiconductor (DMS) materials have been widely studied.[1–19] Compared to other DMS materials, the ZnO-based DMS has a potential advantage for future device applications, which is its above-room-temperature Curie temperature (T_C), according to the calculations of Dietl *et al.*[20] However, unlike GaAs:Mn (Ref. 21) and InAs:Mn (Ref. 22) DMSs, the mechanism and origin of the ferromagnetism in ZnO-based DMSs are still controversial and need further clarification. Very recently, the focus of ZnO DMS research has shifted from achieving room-temperature ferromagnetism in ZnO to understanding the mechanism of ferromagnetism and whether it originates from intrinsic carrier mediation or extrinsic clustering/phase segregation. Recently, Yang *et al.*[19] observed ferromagnetism in *n*-type ZnO:Mn thin films with a T_C above room temperature, and the magnetization shows a monotonic dependence on the electron carrier concentration (n). These results are surprising because Mn-doped ZnO was theoretically predicted to be ferromagnetic only in a hole-rich environment.[20,23] So additional characterizations and analyses, such as systematic microstructure and magnetotransport studies, were performed on ZnO:Mn DMS thin films to further investigate and clarify the origin of the ferromagnetism. In this paper, results from transmission electron microscopy (TEM) studies, magnetoresistance (MR), and Hall effect on ZnO:Mn thin film samples are comprehensively discussed.

[a)]Author to whom correspondence should be addressed. Electronic mail: jianlin@ee.ucr.edu.

II. EXPERIMENT

The ZnO:Ga thin films were grown on *r*-cut sapphire substrates using plasma-assisted molecular-beam epitaxy. Regular Knudsen effusion cells filled with elemental Zn (6N) and Ga (6N) were used as zinc and gallium sources. A radiofrequency plasma supplied with O_2 (5N) was used as the oxygen source. The purpose of Ga incorporation is to tune the electron carrier concentration in ZnO.[24] The substrate temperature was held constant at 565 °C during the growth. After the growth, the samples were annealed *in situ* in vacuum at 800 °C for 20 min to activate the Ga dopants and improve crystallinity. Mn ions were implanted into the as-grown ZnO:Ga thin films with a dose of 3×10^{16} cm^{-2} using an implantation energy of 50 keV. All the Mn-implanted ZnO samples were annealed at 900 °C for 5 min in nitrogen after implantation. Typical Mn-implanted ZnO:Ga thin film samples (these samples are referred to as ZnO:Mn in the paper) were used in the microstructure and transport studies in this paper. The thickness of the ZnO:Mn sample used for transport measurements is 470 nm. Other magnetic properties of the ZnO:Mn samples were already reported in Ref. 19.

Transmission electron microscope analysis including selected area electron diffraction (SAED), high-angle annular dark field (HAADF) (*Z*-contrast) images, and x-ray energy dispersive spectroscopy (EDS) were performed using a JEOL 2010F analytical electron microscope equipped with a field emission gun. Further TEM studies, including SAED and EDS, as well as high-resolution TEM (HRTEM) studies, were also carried out using a JEOL JEM-3011 high-resolution electron microscope operated at 300 kV, with a 0.17 nm point-to-point resolution. Cross-sectional TEM specimens were prepared by mechanical grinding, polishing, and dimpling, followed by argon ion milling in a Gatan

 © 2009 American Institute of Physics

Author complimentary copy. Redistribution subject to AIP license or copyright, see http://jap.aip.org/jap/copyright.jsp

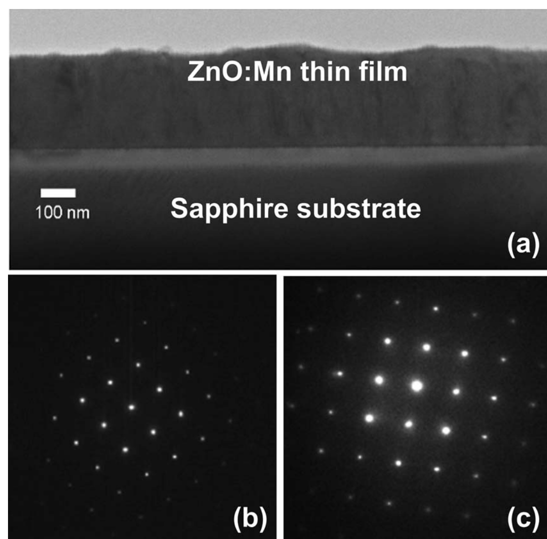

FIG. 1. (a) Cross-sectional TEM image of a ZnO:Mn thin film on a sapphire substrate. (b) A typical SAED pattern from the ZnO:Mn thin film. (c) SAED pattern from the sapphire substrate.

model 691 precision ion polishing system at incident angles between 4.0° and 5.5° to electron transparency. X-ray diffraction (XRD) measurements were performed using a Bruker D8 Advance x-ray diffractometer. MR and field-dependent Hall effect measurements were performed in a Quantum Design physical properties measurement system with magnetic fields up to 10 T. The direction of the magnetic field was perpendicular to the film plane during the MR measurements.

III. RESULTS AND DISCUSSION

A. Structural properties

Figure 1(a) shows a typical cross-sectional TEM image of the ZnO:Mn thin film. The image reveals a relatively low dislocation density, indicating a high-quality film. To investigate the crystallinity and uniformity of the ZnO:Mn thin film, SAED patterns were taken. Figure 1(b) shows a typical SAED pattern of the ZnO:Mn thin film. SAED patterns were also taken at more different locations throughout the ZnO:Mn thin film (not shown here). All the SAED patterns are very similar to each other and lack of any unexpected diffraction spots, indicating a high degree of uniformity and no secondary phases in the ZnO:Mn film. The SAED pattern of the sapphire substrate is shown in Fig. 1(c) for comparison.

HRTEM was performed throughout a wide area of the ZnO:Mn thin film and the film/substrate interface. Typical HRTEM images are shown in Fig. 2(a), Fig. 2(b), Fig. 3(a), and Fig. 3(b), respectively. The zone axes of the film and the substrate are approximately 4° apart from each other, indicating a slight twist between the film and the substrate, but otherwise crystallographic alignment of the ZnO:Mn layer and the sapphire substrate at the interface is good. HRTEM studies indicate also that the film is of high crystallinity and no clustering or secondary phase was observed; however, there are a small number of stacking faults visible.

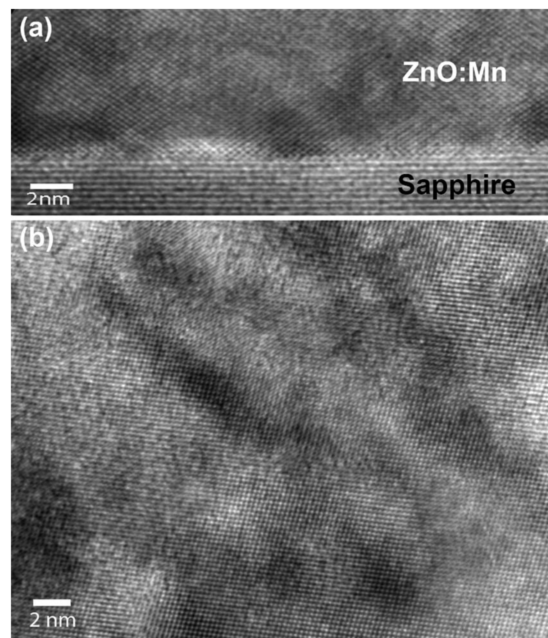

FIG. 2. (a) Cross-sectional HRTEM image of the interface between the ZnO:Mn thin film and the sapphire substrate, showing an atomically sharp interface. (b) HRTEM image of the ZnO:Mn thin film. The film appears to be highly crystalline with no secondary phase.

Figures 3(a) and 3(b) show the HRTEM images from two different areas of the ZnO:Mn thin film. Fast Fourier transform (FFT) patterns were taken on the dark and light areas to examine the uniformity of the film. Figures 3(c)–3(f) show the FFT patterns from the areas indicated in Figs. 3(a) and 3(b). These four FFT patterns are nominally identical, corroborating the evidence from the SAED patterns in indicating that the same crystal structure is present in these areas and that the dark regions are simply contrast variations arising from the stacking faults or the slight variations in specimen thickness.

Conventional HRTEM is a very powerful technique for detecting any possible secondary phases. It is, however, limited by the relatively small region of material that is examined, compared to other techniques. Therefore, HAADF *Z*-contrast imaging was performed to further confirm our conclusion. Figures 4(a) and 4(b) show typical HAADF *Z*-contrast images of the ZnO:Mn thin film. Because in HAADF *Z*-contrast imaging, contrast arises from the atomic number of the elements being probed, it is a powerful and popular technique for detecting and studying embedded nanoparticles or metal ion clusters in films,[25,26] and little contrast arises from sample thickness variation.[25] Larger atomic number element-related phases contribute to brighter contrast.[26] The HAADF *Z*-contrast imaging also shows a much larger region than the HRTEM is able to. No Mn-related segregated phases are detected in all the HAADF images of the ZnO:Mn thin film. The previous conclusion that the film is free of clustering/phase segregation is confirmed by the HAADF *Z*-contrast studies. Dietl *et al.*[27] proposed a model to explain the origin of the ferromagnetism in transition-metal (TM) doped ZnO recently, which assigns the spontaneous magnetization of ZnO:TM to the uncompensated spins at the surface of antiferromagnetic TM-rich

Author complimentary copy. Redistribution subject to AIP license or copyright, see http://jap.aip.org/jap/copyright.jsp

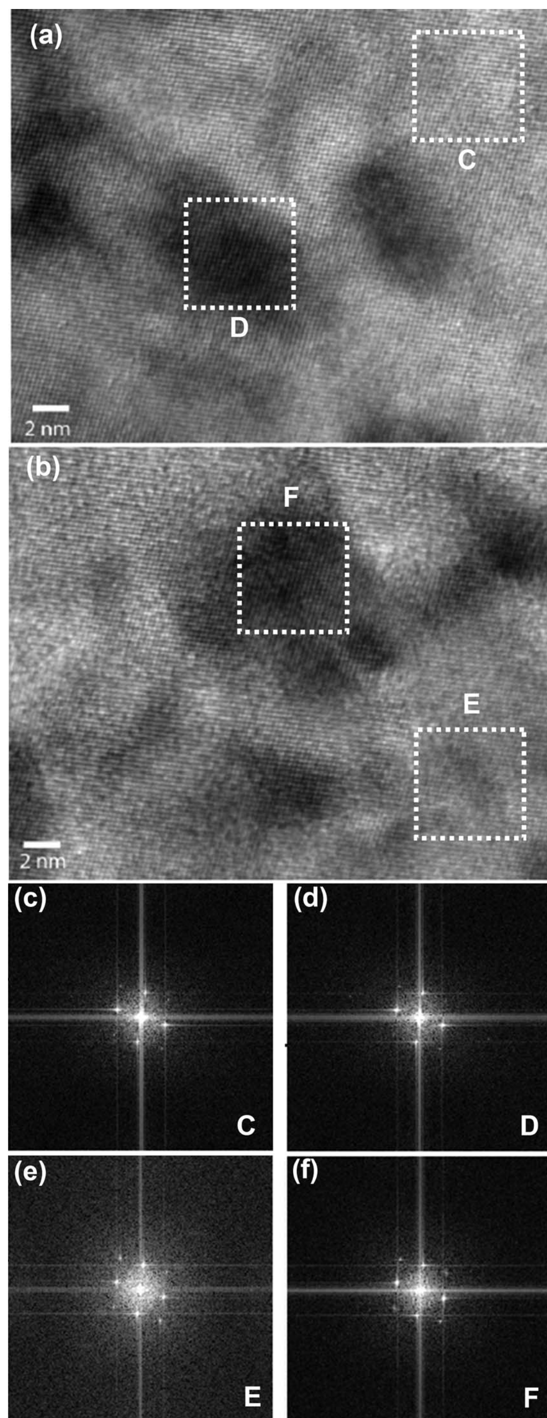

FIG. 3. [(a) and (b)] Two HRTEM images taken from different places on the ZnO:Mn thin film. [(c)–(f)] The FFT patterns corresponding to the square region marked with dotted lines in (a) and (b).

wurtzite (wz) ZnO:TM nanocrystals. These TM-rich wz ZnO:TM nanocrystals are immersed in a TM-poor paramagnetic ZnO:TM matrix. Since the nanocrystals are coherent with identical crystallographic structure and lattice constant to the surrounding ZnO:TM, they escape from the detection of standard HRXRD or HRTEM. HAADF *Z*-contrast images shown here are a good supplementary experimental proof since it brings a better sensitivity and a larger possibility to detect the embedded "coherent" TM-rich ZnO:TM nanocrystals than HRTEM. Within the *Z*-contrast detection limit, no evident signs of Mn-rich ZnO:Mn nanocrystals or Mn spinodal decomposition[28] were observed in the ZnO:Mn film.

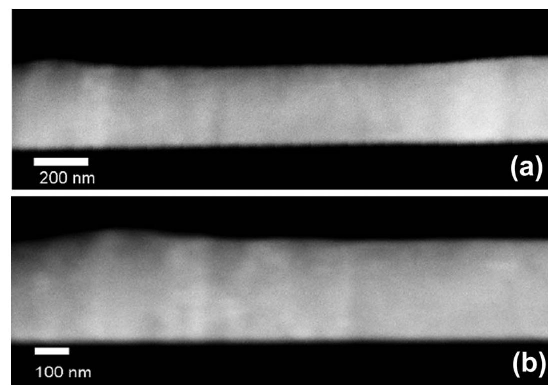

FIG. 4. [(a) and (b)] Two HAADF images of the ZnO:Mn thin film.

Figure 5(a) shows an EDS spectrum from the ZnO:Mn thin film sample. The two strong peaks located at 8.65 and 9.59 keV are the signals from the Zn $K\alpha$ and Zn $K\beta$ shells, respectively. Mn signals are observed at 5.89 and 6.42 keV, which are attributed to Mn $K\alpha$ and Mn $K\beta$ shells, respectively. The inset in Fig. 5(a) shows the electron microscopy image of the region where the EDS measurements were performed. Figure 5(b) shows an XRD pattern for the ZnO:Mn thin film sample. The ZnO:Mn wz $(11\bar{2}0)$ peak was observed at 56.7°, indicating that the growth direction (i.e., the out-of-plane direction) of the ZnO:Mn thin film is along the $[11\bar{2}0]$ direction. The inset shows that the ZnO:Mn $(11\bar{2}0)$ peak has a full width at half maximum (FWHM) of ~0.29°.

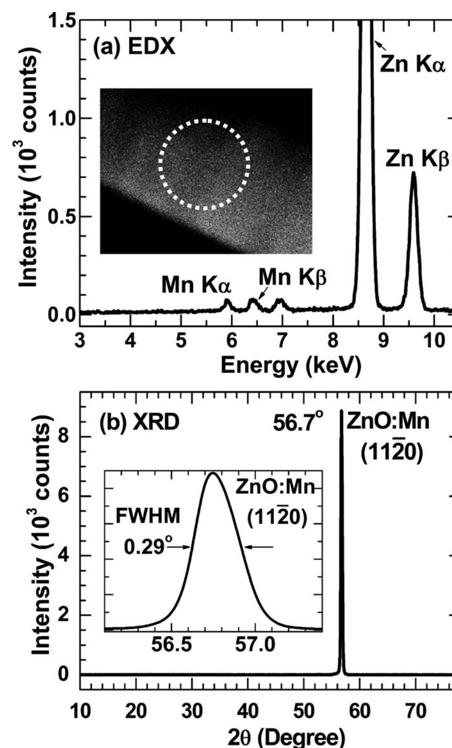

FIG. 5. (a) EDS spectrum of the ZnO:Mn thin film, showing Zn and Mn signals. The inset shows the electron microscopy image of the region where the EDS was taken. (b) XRD pattern of the ZnO:Mn thin film. The orientation of the ZnO:Mn thin film is along the $[11\bar{2}0]$ direction. The inset shows that the FWHM of the $(11\bar{2}0)$ peak located at 56.7° is ~0.29°.

Author complimentary copy. Redistribution subject to AIP license or copyright, see http://jap.aip.org/jap/copyright.jsp

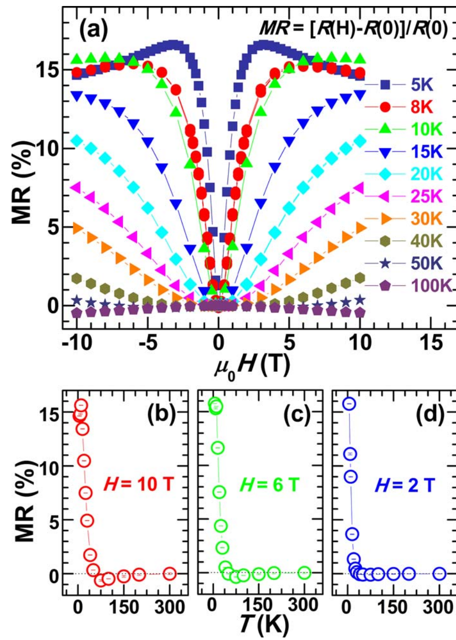

FIG. 6. (Color online) (a) MR of the ZnO:Mn thin film at different temperatures. [(b) and (d)] The temperature dependence of the MR from the ZnO:Mn thin film with applied magnetic fields of 10, 6, and 2 T. The vertical distance between the two thin lines in every circle symbol represents the error bar for that data point. The magnetic field is perpendicular to the film plane for these measurements.

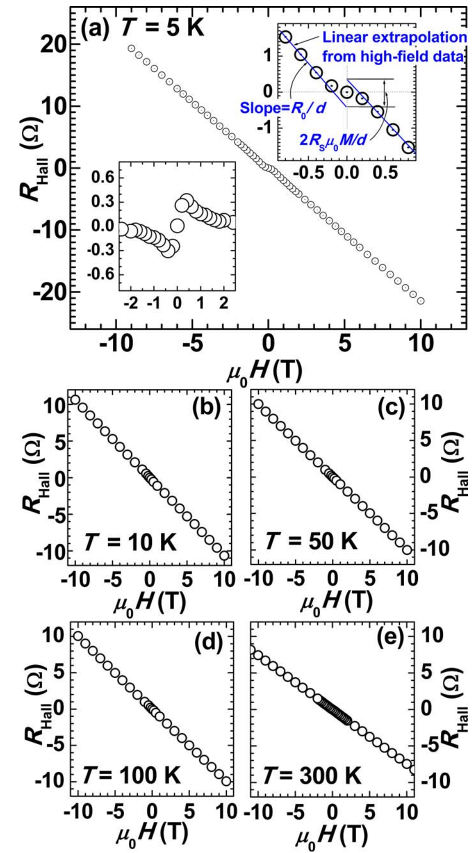

FIG. 7. (Color online) (a) The field dependence of the Hall resistance R_{Hall} measured at 5 K. The linear component of R_{Hall} is from the OHE and the nonlinear contribution to R_{Hall} is from the AHE. The lower inset shows the AHE after subtracting the linear background from the OHE. The upper inset shows the method employed to determine R_0 and R_s. [(b)–(e)] The field dependence of the Hall resistance measured at 10, 50, 100, and 300 K on the same ZnO:Mn thin film sample.

B. Transport properties

Figure 6(a) shows the MR spectra of the ZnO:Mn thin film sample at 5, 8, 10, 15, 20, 25, 30, 40, 50, and 100 K with magnetic fields up to 10 T. The MR is defined as MR $=[R(H)-R(0)]/R(0)$. Figures 6(b)–6(d) show the temperature dependence of the MR measured with magnetic fields of 10, 6, and 2 T. The vertical distance between the two thin lines in every circle symbol represents the error bar for that data point. (The uncertainty is as small as can be comparable to the size of the symbols.) At low temperatures down to 5 K, the MR is large and positive. Initially in weak fields, it quickly increases, and for temperatures from 5 to 10 K, the MR exceeds 15%. Eventually it decreases slightly at higher fields. The MR at 5 K with a field of 3.2 T is 16.6%. As the temperature is increased, the magnitude of the positive MR decreases. A small negative MR component shows up at 50 K, though the MR turns positive at higher fields. For temperatures above this, the MR is small (several percent) and negative over the whole field range. The observed maximum negative MR is -0.63% at 75 K with a field of 10 T. The magnitude of the MR decreases to zero as the temperature further increases until it is insignificant at 300 K. These data indicate a competition between positive and negative contributions to the MR. The positive MR contribution is attributed to the destructive effects on transport of an *sp-d* exchange enhanced *s*-electron splitting in the weakly localized regime,[29–31] which is an indication of the intrinsic ferromagnetism in DMSs. We also found that the positive MR in the ZnO:Mn thin film is much stronger than in the ZnO:Co thin films we prepared with the same conditions.[32] This could be an indication that the *sp-d* exchange coupling in ZnO:Mn is stronger than in ZnO:Co thin films. The negative MR could be from either weak localization, where the magnetic field suppresses quantum constructive interference effect,[33,34] which was also observed in nonmagnetic ZnO thin films,[35] or the field suppression of magnetization fluctuations, leading to the delocalization of bound magnetic polarons.[36]

Figure 7(a) shows the field-dependent Hall resistance for the ZnO:Mn thin film measured at a temperature of 5 K. The vertical axis of the Hall resistance R_{Hall} is defined as the Hall voltage V_H divided by longitudinal current I_x, i.e., $R_{\mathrm{Hall}}=V_H/I_x$. Figures 7(b)–7(e) show the field-dependent Hall effect measurements performed at 10, 50, 100, and 300 K on the same piece of the ZnO:Mn thin film sample.

In magnetic materials, the Hall resistance has two contributions: the ordinary Hall effect (OHE) arising from the classical Lorenz force and the anomalous Hall effect (AHE) due to the asymmetric scattering from the spin-orbit interaction in the presence of a magnetization. So, R_{Hall} is expressed with the following equation:

$$R_{\mathrm{Hall}}=\frac{R_0}{d}(\mu_0 H)+\frac{R_s}{d}(\mu_0 M)\equiv R_{\mathrm{OHE}}+R_{\mathrm{AHE}}, \quad (1)$$

where R_0 and R_{OHE} are the ordinary Hall coefficient and resistance, R_s and R_{AHE} are the anomalous Hall coefficient and resistance, d is the thickness of the ZnO:Mn thin film, which is 470 nm, H and M are the magnetic field and the

Author complimentary copy. Redistribution subject to AIP license or copyright, see http://jap.aip.org/jap/copyright.jsp

TABLE I. Ordinary Hall coefficient R_0, anomalous Hall coefficient R_s, electron carrier concentration n, and resistivity ρ_x at different temperatures.

T (K)	R_0 (10^{-9} Ω cm G^{-1})	n (10^{19} cm^{-3})	R_s (10^{-7} Ω cm G^{-1})	ρ_x (10^{-2} Ω cm)
5	-10.14 ± 0.02	0.616 ± 0.001	3.4 ± 0.5	3.76
10	-5.04 ± 0.01	1.24	2.8 ± 0.2	3.65
50	-4.73 ± 0.01	1.32	1.9 ± 0.2	3.50
100	-4.65 ± 0.01	1.34	1.4 ± 0.2	3.33
300	-3.48 ± 0.05	1.80 ± 0.02	0.3 ± 0.3	2.91

magnetization perpendicular to the film plane, respectively, and μ_0 is the free space permeability. In Fig. 7(a), the linear background with a negative slope is from the OHE. The sign and magnitude of the OHE give information on the carrier type and concentration, respectively. The nonlinear component of R_{Hall} is from the AHE. The lower inset shows the R_{AHE} vs. $\mu_0 H$ spectra after subtracting the linear background (i.e., $R_{\text{Hall}}-R_{\text{OHE}}$), where the AHE is clearly visible. The upper inset shows the method employed to determine R_s. A linear fitting was performed on the high-field data (>5 and <−5 T), where the magnetization is completely saturated. From the slope of the linear fitting R_0/d was found. The distance along the vertical axis between the two intercepts from the extrapolations of the positive and negative high-field fittings is $2R_s\mu_0 M/d$. The magnetization was reported in a previous paper,[19] which shows almost no temperature dependence up to 300 K.

Following the procedure discussed above, R_0 and R_s at different temperatures are listed in Table I. The error bars of R_s are larger than those for R_0 because of the extrapolation of high-field data to zero field axis. Figure 8(a) shows the temperature dependence of R_0. The electron carrier concentration n, which is shown in the inset as function of temperature, for the ZnO:Mn thin film was determined from R_0 using the relation $R_0=-1/ne$, where e is the charge of the electron. The vertical distance between the two thin lines in every circle (R_0) and pentagon (n) symbols represents the error bar of R_0 and n at each temperature point. (The uncertainty is as small as can be comparable to the size of the symbols.) The electron carrier concentration of this ZnO:Mn thin film only changes by a factor of 3 in going from 300 to 5 K, indicating a degenerate semiconductor, which is commonly observed in heavily doped n-type thin films.[24] The values of n at different temperatures are also summarized in Table I. Figure 8(b) shows the temperature dependence of R_s, which decreases with increasing temperature. The observation of an AHE in this ZnO:Mn thin film also provides evidence of intrinsic carrier-mediation ferromagnetism,[37] although the AHE observed here is very weak compared to other ferromagnetic semiconductors, such as GaAs:Mn (Ref. 21) and InAs:Mn.[22] A very small AHE in ZnO-based DMS materials was also reported by others.[30,37–40] The reason is not very clear so far. One of the possible reasons might be the relatively large R_0 in general ZnO thin films due to smaller carrier concentration compared to the GaAs:Mn/InAs:Mn or ferromagnetic metals.

Figure 9 shows the temperature dependence of the resistivity ρ_x of the ZnO:Mn thin film from 2 to 350 K. The inset shows the same data, plotted as a function of reciprocal temperature. The resistivity does not show a strong temperature dependence because of the degenerate carrier statistics of this semiconducting ZnO:Mn thin film. This is consistent with the previous discussion on the temperature dependence of n. The values of ρ_x at 5, 10, 50, 100, and 300 K are also summarized in Table I.

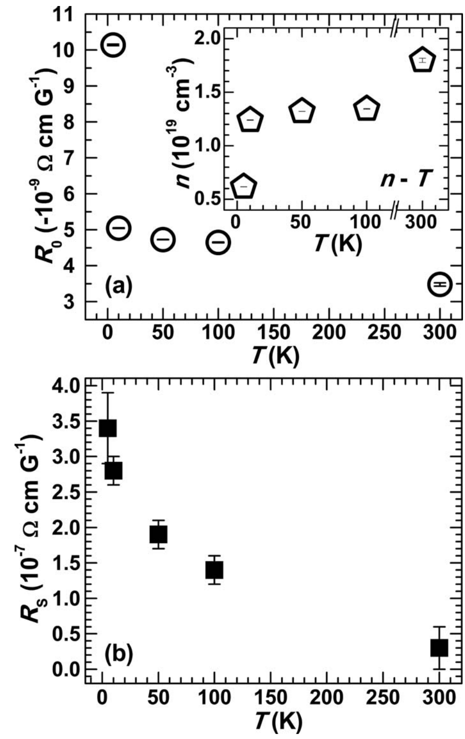

FIG. 8. (a) The temperature dependence of ordinary Hall coefficient R_0. The inset shows the temperature dependence of the electron carrier concentration n derived from R_0. The vertical distance between the two thin lines in every symbol represents the error bar of the data point. (b) The temperature dependence of anomalous Hall coefficient R_s.

The origin of the AHE is attributed to spin-orbit coupling, and R_s depends on ρ_x as $R_s=a_{sk}\rho_x+b_{sj}\rho_x^2$.[41–43] The linear term is physically interpreted as the skew scattering where the angle $\phi_{sk}=a_{sk}\cdot\mu_0 M$ represents the average deflection of a charge carrier at a scattering center. The quadratic term is associated with a side-jump mechanism where the charge carrier's trajectory is displaced a fixed distance perpendicular to its original path at each scattering center. Fig-

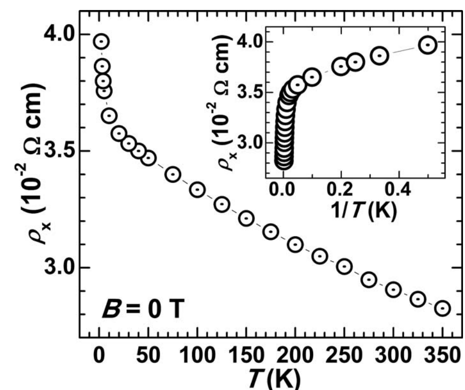

FIG. 9. (a) The temperature dependence of the resistivity ρ_x from 2 to 350 K. The inset shows the same data with reciprocal temperature along the horizontal axis.

Author complimentary copy. Redistribution subject to AIP license or copyright, see http://jap.aip.org/jap/copyright.jsp

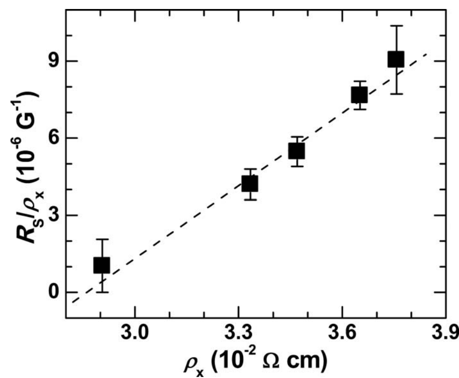

FIG. 10. The relation between R_s/ρ_x and ρ_x. The solid square symbols with error bars are the experimental data. The dashed line shows a linear fit to the data, representing the linear and quadratic dependences of ρ_x on R_s.

ure 10 shows the relation between R_s/ρ_x and ρ_x. The solid square symbols with error bar are the experimental data and the dashed line shows the fit. ϕ_{sk} is estimated to be ~ -0.4 mrad and b_{sj} is approximately $9.4 \times 10^{-4}\ \Omega^{-1}\ \mathrm{cm}^{-1}\ \mathrm{G}^{-1}$. The negative value of ϕ_{sk} is widely observed in ferromagnetic TMs.[44]

IV. SUMMARY

The HRTEM and SAED studies indicate that the ZnO:Mn DMS thin film is of high-quality, uniform, and free of clustering/segregated phases. *Z*-contrast imaging and XRD further corroborate the absence of phase segregation in the film, leading us to believe that the ferromagnetism in this material is intrinsic. A large positive MR is observed, indicating a strong *sp*-*d* exchange in ZnO:Mn DMS thin films. Both the ordinary and anomalous Hall coefficients were determined from the field dependence of Hall resistance. The anomalous Hall coefficient has a strong quadratic dependence on the resistivity, which implies a side-jump scattering mechanism in the AHE, further supporting the origin of the ferromagnetism in ZnO:Mn DMS thin films.

ACKNOWLEDGMENTS

This work was supported by ONR/DMEA through the Center of Nanomaterials and Nanodevices (CNN) under Award No. H94003-08-2-0803. Electron microscopy studies at the Electron Microbeam Analysis Laboratory at the University of Michigan were supported by the National Science Foundation under Grant Nos. DMR-0315633 and DMR-9871177.

[1]S. J. Pearton, W. H. Heo, M. Ivill, D. P. Norton, and T. Steiner, Semicond. Sci. Technol. **19**, R59 (2004).
[2]C. Liu, F. Yun, and H. Morkoç, J. Mater. Sci.: Mater. Electron. **16**, 555 (2005).
[3]T. Fukumura, Z. Jin, A. Ohtomo, H. Koinuma, and M. Kawasaki, Appl. Phys. Lett. **75**, 3366 (1999).
[4]T. Fukumura, Z. Jin, M. Kawasaki, T. Shono, T. Hasegawa, S. Koshihara, and H. Koinuma, Appl. Phys. Lett. **78**, 958 (2001).
[5]K. Ando, H. Saito, Z. Jin, T. Fukumura, M. Kawasaki, Y. Matsumoto, and H. Koinuma, Appl. Phys. Lett. **78**, 2700 (2001).
[6]K. Ueda, H. Tabata, and T. Kawai, Appl. Phys. Lett. **79**, 988 (2001).
[7]Z. Jin, T. Fukumura, M. Kawasaki, K. Ando, H. Saito, T. Sekiguchi, Y. Z. Yoo, M. Murakami, Y. Matsumoto, T. Hasegawa, and H. Koinuma, Appl. Phys. Lett. **78**, 3824 (2001).
[8]H. J. Lee, S. Y. Jeong, C. R. Cho, and C. H. Park, Appl. Phys. Lett. **81**, 4020 (2002).
[9]D. P. Norton, M. E. Overberg, S. J. Pearton, K. Pruessner, J. D. Budai, L. A. Boatner, M. F. Chisholm, J. S. Lee, Z. G. Khim, Y. D. Park, and R. G. Wilson, Appl. Phys. Lett. **83**, 5488 (2003).
[10]P. Sharma, A. Gupta, K. V. Rao, J. Frank, F. R. Owens, R. Sharma, R. Ahuja, J. M. Osorio Guillen, B. Johansson, and G. A. Gehring, Nature Mater. **2**, 673 (2003).
[11]D. A. Schwartz and D. R. Gamelin, Adv. Mater. (Weinheim, Ger.) **16**, 2115 (2004).
[12]M. Venkatesan, C. B. Fitzgerald, J. G. Lunnery, and J. M. D. Coey, Phys. Rev. Lett. **93**, 177206 (2004).
[13]J. M. D. Coey, M. Venkatesan, and C. B. Fitzgerald, Nature Mater. **4**, 173 (2005).
[14]M. H. F. Sluiter, Y. Kawazoe, P. Sharma, A. Inoue, A. R. Raju, C. Rout, and U. V. Waghmare, Phys. Rev. Lett. **94**, 187204 (2005).
[15]K. R. Kittilstved, N. S. Norberg, and D. R. Gamelin, Phys. Rev. Lett. **94**, 147209 (2005).
[16]K. R. Kittilstved, D. A. Schwartz, A. C. Tuan, S. M. Heald, S. A. Chambers, and D. R. Gamelin, Phys. Rev. Lett. **97**, 037203 (2006).
[17]C. Song, K. W. Geng, F. Zeng, X. B. Wang, Y. X. Sheng, F. Pan, Y. N. Xie, T. Liu, T. T. Zhou, and Z. Fan, Phys. Rev. B **73**, 024405 (2006).
[18]H. Pan, J. B. Yi, L. Shen, R. Q. Wu, J. H. Yang, J. Y. Lin, Y. P. Feng, J. Ding, L. H. Van, and J. H. Yin, Phys. Rev. Lett. **99**, 127201 (2007).
[19]Z. Yang, J. L. Liu, M. Biasini, and W. P. Beyermann, Appl. Phys. Lett. **92**, 042111 (2008).
[20]T. Dietl, H. Ohno, F. Matsukura, J. Cibert, and D. Ferrand, Science **287**, 1019 (2000); T. Dietl, H. Ohno, and F. Matsukura, Phys. Rev. B **63**, 195205 (2001).
[21]H. Ohno, Science **281**, 951 (1998).
[22]H. Ohno, D. Chiba, F. Matsukura, T. Omiya, E. Abe, T. Dietl, Y. Ohno, and K. Ohtani, Nature (London) **408**, 944 (2000).
[23]K. Sato and H. Katayama-Yoshida, Semicond. Sci. Technol. **17**, 367 (2002).
[24]Z. Yang, D. C. Look, and J. L. Liu, Appl. Phys. Lett. **94**, 072101 (2009).
[25]M. Shiojiri and H. Saijo, J. Microsc. **223**, 172 (2006).
[26]S. Utsunomiya and R. C. Ewing, Environ. Sci. Technol. **37**, 786 (2003).
[27]T. Dietl, T. Andrearczyk, A. Lipińska, M. Kiecana, M. Tay, and Y. Wu, Phys. Rev. B **76**, 155312 (2007).
[28]S. Kuroda, N. Nishizawa, K. Takita, M. Mitome, Y. Bando, K. Osuch, and T. Dietl, Nature Mater. **6**, 440 (2007).
[29]J. Wang, Z. Gu, M. Lu, D. Wu, C. Yuan, S. Zhang, Y. Chen, S. Zhu, and Y. Zhu, Appl. Phys. Lett. **88**, 252110 (2006).
[30]Q. Xu, L. Hartmann, H. Schmidt, H. Hochmuth, M. Lorenz, R. Schmidt-Grund, D. Spemann, and M. Grundmann, J. Appl. Phys. **100**, 013904 (2006).
[31]M. Sawicki, T. Dietl, J. Kossut, J. Igalson, T. Wojtowicz, and W. Plesiewicz, Phys. Rev. Lett. **56**, 508 (1986).
[32]Z. Yang, M. Biasini, W. P. Beyermann, M. B. Katz, O. K. Ezekoye, X. Q. Pan, Y. Pu, J. Shi, Z. Zuo, and J. L. Liu, J. Appl. Phys. **104**, 113712 (2008).
[33]P. A. Lee and V. Vramakrishnan, Rev. Mod. Phys. **57**, 287 (1985).
[34]S. Hikami, A. I. Larkin, and Y. Nagaoka, Prog. Theor. Phys. **63**, 707 (1980).
[35]A. Goldenblum, V. Bogatu, T. Stoica, Y. Goldstein, and A. Many, Phys. Rev. B **60**, 5832 (1999).
[36]H. Ohno, H. Munekata, T. Penney, S. von Molnar, and L. L. Chang, Phys. Rev. Lett. **68**, 2664 (1992).
[37]Y. Z. Peng, T. Liew, T. C. Chong, C. W. An, and W. D. Song, Appl. Phys. Lett. **88**, 192110 (2006).
[38]Q. Xu, L. Hartmann, H. Schmidt, H. Hochmuth, M. Lorenz, R. Schmidt-Grund, C. Sturm, D. Spemann, and M. Grundmann, Phys. Rev. B **73**, 205342 (2006).
[39]Q. Xu, L. Hartmann, H. Schmidt, H. Hochmuth, M. Lorenz, R. Schmidt-Grund, C. Sturm, D. Spemann, M. Grundmann, and Y. Liu, J. Appl. Phys. **101**, 063918 (2007).
[40]S. J. Pearton, D. P. Norton, M. P. Ivill, A. F. Hebard, J. M. Zavada, W. M. Chen, and I. A. Buyanova, IEEE Trans. Electron Devices **54**, 1040 (2007).
[41]R. C. O'Handley, *Modern Magnetic Materials: Principles and Applications* (Wiley, New York, 2000), pp. 570–573.
[42]C. M. Hurd, *The Hall Effect in Metals and Alloys* (Plenum, New York, 1972), Chap. 5.
[43]C. L. Chien and C. W. Westgate, *The Hall Effect and Its Applications* (Plenum, New York, 1980).
[44]E. P. Wohlfarth, *Ferromagnetic Materials*, edited by I. A. Campbell and A. Fert (North-Holland, Amsterdam, 1982), Vol. 3, Chap. 9.

Author complimentary copy. Redistribution subject to AIP license or copyright, see http://jap.aip.org/jap/copyright.jsp